Improved Surface Gravity and Mass Constraints for Substellar Objects from Spectral Line Profile Measurements at High Resolution in the Near-Infrared

JESSICA J. SPEEDIE[1], DAVID LAFRENIERE[2]

1. Integrated Science Program, Class of 2020, McMaster University
2. Institut de Recherche sur les Exoplanètes, Département de Physique, Université de Montréal

SUMMARY

Observed extra-solar systems within the Milky Way are comprised of stars and substellar objects (planets and brown dwarfs). Standard methods for measuring the mass of isolated brown dwarfs and directly-imaged giant planets are indirect, and rely heavily on largely uncalibrated theoretical models. Consequently, current mass estimates for many of these substellar objects are highly uncertain. With the arrival of new high resolution instruments such as SPIRou comes opportunity for new methods and improved constraints. We present an observational method to constrain the mass of substellar objects precisely, and demonstrate its feasibility on simulated SPIRou observations. We use a cross correlation technique to find the average shape of the absorption lines in an object's spectrum, and determine its surface gravity to high precision through quantitative comparison to reference models. The average line profile width has the properties of being dependent on surface gravity and independent on the choice of reference model. Our results suggest that by using the average line profile, surface gravity can be constrained to better than 5%, and mass can subsequently be estimated to a precision of 10-15%. Performing our method on real high-resolution observations will provide the ultimate test.

Received: 11/09/2018 **Accepted:** 02/14/2019 **Published:** 11/17/2019

Keywords: brown dwarfs: atmospheres - line profiles - methods: observational - planets and satellites: individual (2MASS 2322-6151)

INTRODUCTION

To know the mass of an object in the sky is to know its nature. Astronomers classify most astronomical bodies into planets, brown dwarfs, or stars depending on how massive they are. Brown dwarfs and planets are not massive enough to sustain nuclear reactions in their cores, and as such are deemed "substellar." The environment in which a planet, a brown dwarf or a star can be found is of great interest for understanding the formation and evolution of the diverse celestial population.

For example, discovering a sub-stellar object (a giant planet or a brown dwarf) *in isolation* indicates it may have actually formed how a star does. The mass distribution of the isolated objects is called the initial mass function, and the lower end of the distribution is the focus of much research. On the other hand, the mass distribution of *companion* objects, those that orbit a star, can answer questions about the formation and evolution of an

astronomical system. Mass as a function of separation of host star, known as the population demographics of companion objects, serves as input for theories concerning the interactions between the bodies in a single system over time. Planets may migrate toward or away from their star, gravitationally scatter off one another, and have observable effects on the circumstellar disks from which they formed. Mass is the key piece of information necessary for insight into all of these processes.

However, it is difficult to determine the mass of substellar objects, and many of the estimates currently available for known directly-imaged giant planets and brown dwarfs (both isolated and companion) are uncertain. Mass cannot be measured directly, and is generally estimated based on an object's observed luminosity and age, in comparison to what theoretical evolution and spectral models predict. It is possible, in the case of binary systems, to measure the mass of substellar objects more precisely using dynamics (Bowler et al., 2018; Dupuy et al., 2018; Dupuy & Liu, 2017). However, the method applies more easily to heavier objects and does not serve as a general one.

Both evolution and spectral models, on which most mass estimates are based, carry significant uncertainties. The initial conditions for the formation of a brown dwarf or giant planet pertinent for evolution models are unconstrained observationally; the energy transferred to a protoplanet by infalling gas may be fully retained (the "hot-start" scenario) or it may be shocked back into space (the "cold-start" scenario), depending on the physics of accretion (Burrows et al., 1997; Marley et al., 2007; Szulágyi & Mordasini, 2016). The subsequent evolution of an object's observable properties after a "hot-start" is quite different to that after a "cold start". This introduces large uncertainties when using evolution models to infer properties such as mass for an object of a given age based on how it is observed today. Uncertainties in spectral models, on the other hand, originate from incorrectly modelling the physics in the atmosphere. Whatever the amount of heat trapped in the interior from formation may be, it will escape through the atmosphere in the form of radiation. Creating spectral models of the emergent radiation is a difficult task due to the complex interactions between molecules in the atmosphere, and the unknown formation or spatial distribution of dust grains and clouds (Homeier et al., 2004).

The uncertainties in the spectral and evolution models that result for the reasons given above are translated into uncertainties in mass estimates by the use of methods that rely heavily on their accuracy. To give examples of a few giant planets or brown dwarfs with poorly constrained masses, we quote the best currently available mass estimates. ROXs 12 b is 12-20 Jupiter masses (Santamaría-Miranda et al., 2018); 51 Eri b: 2-12 M_{Jup} (Rajan et al., 2017); CT Cha B: 14-24 M_{Jup} (Wu et al., 2015); 2MASS 0103+1935: 12.82 ± 8.43 M_{Jup} (Faherty et al., 2016). Notably, since the dividing-line between a planet and a more massive brown dwarf is 13 M_{Jup}, it happens that astronomers don't confidently know what these objects truly are.

In this work, we aim to ameliorate this situation, with the help of new technology. We demonstrate an observational method that can be applied generally for constraining the mass of substellar objects more tightly than methods that rely on evolution models, using high resolution near-infrared spectroscopy. We present our method in the context of the Canada-France-Hawaii Telescope's new high resolution (R=73,500) IR spectrograph: SPIRou. This revolutionary instrument became operational in mid-2018, and it is only with high resolution spectra from instruments like SPIRou that our method is possible.

We take the approach of first determining the object's surface gravity, and subsequently using it to find the mass. It is well known that the thermal emission spectrum is sensitive to surface gravity (Hedges & Madhusudhan, 2016; Cruz et al., 2009a). Many previous works have estimated surface gravity using low resolution spectroscopic observations by comparison with models (Schneider et al., 2016; Chilcote et al., 2015; Bonnefoy et al., 2014; Currie et al., 2013; Bonnefoy et al., 2010); however, the resulting accuracy is seldom better than 0.5-1.0 dex.* Our method uses the information afforded by the high resolution of instruments like SPIRou, namely the line profile of thousands of individual molecular lines, to

* The term "dex" is often used by astrophysicists as a shorthand for "order of magnitude." For example, 0.1 dex $\equiv 10^{5.1} - 10^{5.0}$, where "5" could be any number, and the difference would still be 0.1 dex.

constrain the surface gravity more precisely. From this, we obtain a correspondingly precise estimate of the mass.

In the following section, we describe our observational method, the collection of spectral models we use, and our process for creating simulated SPIRou observations. We then introduce the Average Line Profile, describe how it can be quantified, and demonstrate its two crucial properties. Next, we perform our method on simulated SPIRou observations of a real object, 2M 2322-6151, and present the mass uncertainty obtained. Finally, we discuss implications, limitations and future work.

METHODS

ANALYSIS APPROACH

The mass of a brown dwarf (or any self-luminous astronomical object) can be expressed as a function of only three properties: its effective temperature, its luminosity and its surface gravity. There already exist precise methods of determining the effective temperature and luminosity, and it is our hope to provide a robust determination technique for the surface gravity.

The strength of the gravitational field on the surface of an astronomical object, g in cm s^{-2} (often quoted as $\log_{10}(g)$), is stronger for denser objects and weaker for less dense objects. It is defined as:

$$g = \frac{Gm}{r^2}\,, \qquad (1)$$

where G is the gravitational constant, m is the object's mass and r is its radius.

An object's luminosity, the amount of energy it emits per unit time, is a basic observable quantity and depends on its surface area and effective temperature:

$$L = 4\pi r^2 \sigma T_{\rm eff}^4\,, \qquad (2)$$

where σ is the Stefan-Boltzmann constant. Equating the radii terms in Equations 1 and 2 yields an object's mass as a function of those aforementioned three properties:

$$m = \frac{1}{4\pi G\sigma}\frac{L}{T^4}g\,. \qquad (3)$$

The uncertainty associated with a given mass measurement, dm, thus depends on the precision with which luminosity, temperature and surface gravity are known. Expressed as a fraction of the mass measurement, we find

$$\frac{dm}{m} = \sqrt{\left(\frac{dg}{g}\right)^2 + \left(\frac{dL}{L}\right)^2 + 16\left(\frac{dT}{T}\right)^2}\,, \qquad (4)$$

which we obtained from the usual simple variance formula.

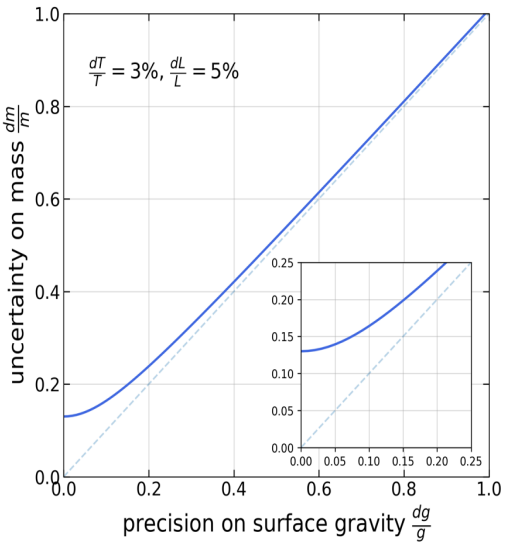

Figure 1: The fraction uncertainty in mass as a function of the fraction uncertainty in surface gravity (given by Equation 4) for the case where temperature and luminosity are known to a precision of 3% and 5%, respectively. A low uncertainty in surface gravity yields a nearly equally low uncertainty in mass (with diminishing returns after a point). The one-to-one line (*dashed*) is shown for reference. *Inset*: Constraints on temperature and luminosity tighter than the 3% and 5% used to create the track shown would be necessary in order to reach a precision on mass better than 13%. **Main point**: If the surface gravity of a brown dwarf or giant planet can somehow be determined and well constrained, then the object's mass can in turn be found to a precision that is only slightly worse.

We can estimate the potential rewards of our approach by calculating the uncertainty in mass for varying constraints on luminosity, temperature and surface gravity. Figure 1 shows the relative uncertainty in mass as a function of how precisely surface gravity is known, for the hypothetical scenario wherein luminosity and temperature are known to a commonly-achieved precision of 5% and 3%, respectively. A tighter constraint on an object's surface gravity yields a tighter constraint on its mass. If the log(g) of a giant planet with mass M = 10 M_{Jup} could somehow be determined to a precision of, for example, 10%, then the uncertainty with which its mass could be known would be ± 16%, or ± 1.6 M_{Jup}, a tight constraint compared to many current estimates quoted in the literature.

SOURCING THERMAL EMISSION SPECTRA

An object's atmospheric conditions determine the features present in its thermal emission spectrum, including the shape of the continuum and the shape of molecular absorption lines. The purpose of atmosphere models is to describe the features produced under given conditions, so that we can understand the observations, and predict what is observable.

We consider here two different sets of brown dwarf thermal emission models: the publically available precomputed grid of PHOENIX BT-SETTL atmosphere models (Allard et al., 2011) and the unpublished atmosphere models of Tremblin et al. (2015, 2016). We have sourced eight of the former (at two temperatures and four surface gravities) and have access to only four of the latter (at two temperatures and two surface gravities). Table 1 outlines their respective properties.

As the premise of this paper is to demonstrate the feasibility of an observational technique, we consider the Tremblin et al. (2015) spectral models to describe the atmosphere of a hypothetical, illustrative target brown dwarf. We employ the PHOENIX BT-SETTL models to be our set of "reference models", for no reason other than that they are available in a more comprehensive range of temperatures and surface gravities.

The biggest difference between the models is the treatment of clouds. PHOENIX BT-SETTL models use a parameter-free cloud model to account for dust formation (following Rossow, 1978) and incorporate microphysical atmospheric processes such as settling of dust under the influence of gravity. The Tremblin et al. (2015) models are cloud-less. Designed to reproduce reddening in cold T and Y dwarfs, they incorporate vertical mixing, quenching of ammonia and a slightly reduced temperature gradient in the atmosphere.

Table 1: Properties of our reference models (denoted with [a], Allard et al., 2012) and notional brown dwarf models (denoted with [b], Tremblin et al., 2015): local thermodynamic equilibrium (LTE); effective temperature (T_{eff}); surface gravity ($\log_{10}g$); spectral resolution (R); metallicity by $\log_{10}$ number density with respect to solar values ([M/H]).

	PHOENIX BT-Settl [a]	Tremblin [b]
Local Equil-ibrium	Thermal	Chemical
T_{eff} (K)	900, 1000	900, 1000
$\log_{10}(g)$	4.0, 4.5, 5.0, 5.5	4.0, 5.0
R	99,406	338,616
[M/H]	0.0	0.0
Source	https://phoenix.ens-lyon.fr/	Personal commun-ication

CREATING SIMULATED SPIRou OBSERVATIONS

We create simulated SPIRou observations of model spectra, specifically the Tremblin et al. (2015) illustrative models, by mimicking two key processes:

1. The interaction of the target's light with Earth's atmosphere on its journey to the telescope;

2. The behaviour of the photons within the observing instrument.

The Earth's atmosphere absorbs light coming to us from the object we want to observe. The effect it has on observations is known as telluric absorption, and needs to be corrected for. We simulate the effect of telluric absorption by

multiplying our target model spectrum with the TAPAS model telluric spectrum (Bertaux et al., 2014), compounded by airmass:

$$F_{obs}(\lambda) = T^{a}(\lambda) F_{int}(\lambda)\,, \qquad (5)$$

where F_{int} is the target's intrinsic spectrum before passing through Earth's atmosphere, F_{obs} is what enters the telescope to be observed, T is the telluric spectrum ($\in [0,1]$) raised to the power of a, which represents the airmass* at the time and location of observation (taken to be 1, for ideal conditions). We oversample the target model spectrum to the resolution of the TAPAS model (R= $\lambda/d\lambda$~ 960,000, where $d\lambda$ is one spectral resolution element) before multiplication in order to best approximate the resolution at which telluric absorption occurs in reality (theoretically infinite).

When propagated through a telescope and spectrograph, a target's photons are diffracted, resulting in monochromatic peaks registering on the detector over a range of wavelengths as broader distributions. The smallest wavelength interval separating two lines that SPIRou can resolve as such, known as 1 resolution element, is 4.1 km s^{-1} and corresponds to 2 pixels on the detector. We mimic this process by convolving the telluric-multiplied target model spectrum to the line spread function (LSF) of SPIRou, for which we use a Gaussian with FWHM equal to one resolution element. We then interpolate the value of the convolved spectrum onto a new vector of wavelength pixels that represents the resolution of the instrument (R=73,500). Photon noise is the main source of uncertainty in the signal (scaling like its square root), though we include dark noise and read-out noise as well.

Finally, we make efforts to emulate the correction process undertaken for real observations, namely telluric correction. We divide the simulated observation and the associated noise of each flux value by the aforementioned TAPAS model, resampled onto the same wavelength pixels. We discard those regions of the target spectrum of low flux and high telluric absorption where the resulting flux and associated noise blow up (around 1.4 and 1.8 μm), leaving us with fewer spectral lines than are present in the full spectrum.

FINDING THE AVERAGE ABSORPTION LINE PROFILE

The high resolution of the observed spectra provided by spectrographs like SPIRou (R = 73,500) gives opportunity for creativity and should be exploited fully. The molecular absorption line width for a slow-rotating (period ~ 12 h; Artigau, 2018) brown dwarf of 1 R_{Jup}, roughly 10 km s^{-1}, is well within SPIRou's capability to resolve.

Surface gravity influences the ambient atmosphere conditions and thus, the absorptive behaviour of the molecules. The wide spectral interval of SPIRou (0.94 - 2.35 μm) enables us to view many thousands of spectral absorption lines, which we can then combine to create a single average absorption profile.

We create our average line profiles by cross correlating the spectra with an artificially constructed "stick spectrum" - a mask. Figure 2 demonstrates the process, which is described below.

1. We begin with a set of reference model spectra of four different surface gravities. We resample (ie. convolve and interpolate) each spectrum to common wavelength pixels, if necessary, or to those of the observing instrument.

2. Fit an akima spline function to each spectrum over wavelength regions excluding absorption lines to find its "pseudo-continuum" (roughly speaking, the large-scale behaviour of the spectrum).

3. Normalize every spectrum by its respective pseudo-continuum to obtain solely the absorption lines.

4. Define an array of zeroes on the common wavelength pixels (to become the stick spectrum).

5. Identify the local minima in flux of the spectrum in the set of lowest surface gravity ($F_{min}^{\log(g)=4.0}$) and set the value of the stick spectrum at those wavelength pixels to 1 (or any non-zero constant).

6. Reject those sticks where the absorption lines of each spectrum do not demonstrate different behaviour as a function of surface gravity. In our case, we keep the sticks at those wavelength pixels

* Airmass is a measure of the amount of Earth atmosphere traversed by the incoming light given the object's elevation in the sky. It is largest on the horizon and at a minimum directly overhead.

where $F_{min}^{\log(g)=4.0} < F_{min}^{\log(g)=4.5} < F_{min}^{\log(g)=5.0} < F_{min}^{\log(g)=5.5}$ and set the rest to zero.

7. Convolve the stick spectrum with a Gaussian profile of σ=2.

8. Cross correlate each spectrum with the stick spectrum individually, in doppler shift space (ie. as a function of radial velocity), from -50 to +50 km s^{-1}.

9. Normalize the resulting cross correlation functions to be between 0 and 1 (ie. $(y_i = y_i - y_{min}) / (y_{max} - y_{min})$) to obtain their absolute shape.

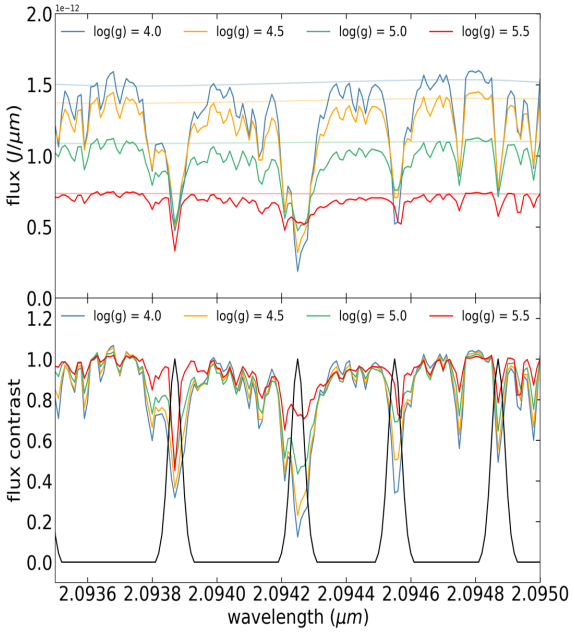

Figure 2: *Top*: Four of the PHOENIX BT-SETTL reference model spectra (at 1000K) and their respective pseudo-continua (pale colours) over a small portion of the SPIRou wavelength interval. *Bottom*: The same four model spectra, pseudo-continuum normalized, and the Gaussian sticks yielded by our algorithm in that region (black). **Main point**: Our algorithm for computing the average line profile for a given set of reference model spectra involves cross correlating an artificially constructed stick spectrum with the spectra's absorption lines.

Constructing the stick spectrum is more of an art than a science, and the resulting cross correlation functions are highly sensitive to the chosen requirements. However, since we cross correlate each model spectrum to the same stick spectrum, the generated CCFs can be meaningfully compared and we are at liberty to impose any criteria.

We compute the cross correlation values at increments in radial velocity of 20 m s^{-1}, which yields an effective resolution of $R = c/\Delta v$ = 15,000,000. With this method, we can effectively probe the average line profile of a spectrum at a much higher resolution than that with which we actually observe it.

RESULTS: THE AVERAGE LINE PROFILE

In this section we apply our cross correlation algorithm described in Section 2.4 to the reference (PHOENIX BT-SETTL) and illustrative (Tremblin et al., 2015) model thermal emission spectra, at their original resolution. This is done in order to understand what is possible to achieve in theory, and what the observations can aim for.

QUANTIFYING THE AVERAGE LINE PROFILE

We present the resulting average line profile yielded by our cross correlation algorithm for one of the eight PHOENIX BT-SETTL reference model spectra in Figure 3. In an effort to quantifiably distinguish between the average line profiles of atmospheres at different surface gravities, we tried to fit them with functions whose shape resemble those of spectral absorption lines - namely a Gaussian, Lorentzian and Voigt profile. In addition to their parameters of characteristic width (σ, γ, and both σ and γ, respectively), we employ a horizontal stretch (s) and a vertical translation factor (lift, l). We find that the best fit to the average line profiles is given by the Lorentzian function centered about x=0:

$$Lor(x, \gamma, s, l) = \frac{\gamma/\pi}{(sx)^2 + \gamma^2} + l\,, \qquad (6)$$

where x is radial velocity in km s^{-1} and γ is the HWHM of Lor(x, γ), ie. what the half width at half maximum would be without the added parameters of stretch and lift. Therefore, it is necessary to set

the function to half its maximum value, $\frac{1}{2}(\frac{1}{\pi\gamma}+l)$, and solve for the characteristic width, in km s^{-1}:

$$w = \pm\sqrt{\frac{\pi\gamma^3 l + \gamma^2}{s^2(1-\pi\gamma l)}}. \qquad (7)$$

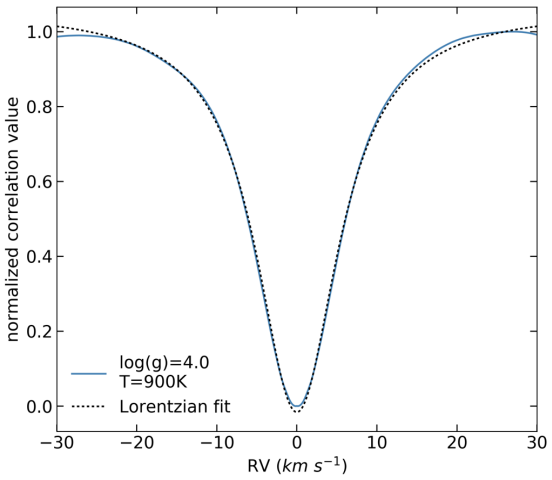

Figure 3: An average line profile, given by our cross-correlation method, and its Lorentzian fit given by Equation 6. The fit quality of the other seven BT-SETTL reference models is similar. This line profile represents the average shape of, in this case, 2736 individual spectral absorption lines. **Main point**: A Lorentz profile (upside-down and vertically translated) describes the average line profile well.

Table 2 presents these values for each model spectrum shown in Figure 3.

PROPERTIES OF THE AVERAGE LINE PROFILE

As is apparent numerally in Table 2 and visually in Figure 4, the width of the average line profile is dependent on surface gravity. The trend suggests that atmospheres at lower surface gravities exhibit narrower absorption lines, on average, while the molecular lines of atmospheres at higher surface gravities tend to be broader.

This result is indeed entirely contrived by our algorithm (which selects only those absorption lines obeying the marching order with surface gravity); however, consider the physical processes occurring on the molecular level in a brown dwarf or giant planet atmosphere, and how they depend on the strength of the gravitational field. Higher surface gravity would lead to increased ambient pressure and temperature, resulting in collisional and thermal broadening of molecular absorption lines in the object's emission spectrum. In this sense, step 6 of our algorithm (Section 2.4) is not arbitrary – in fact, therein lies the method's utility and merit. Enough absorption lines in the reference model spectra (roughly 2500) follow the trend such that the resulting average line profiles are clearly differentiated. Thus, the set can be used as a reference basis, against which one can compare the average line profile of an observed object whose surface gravity is unknown. Provided that the average line profiles of both the observed spectrum and model spectra are created using the exact same stick spectrum, the observed object's surface gravity can be determined relative to that of the reference models.

Table 2: Characteristic widths (given by Equation 7, in km s^{-1}) for the Lorentzian fits to each of the eight reference and four illustrative model spectra. Quoted uncertainties are for $x(\gamma, s) = \gamma/s$, not $x(\gamma, s, l)$ (= Equation 7), because the former yielded higher uncertainties.

	log(g)	900 K	1000 K
BT-Settl (reference models)	4.0	5.71 ± 0.02	5.96 ± 0.02
	4.5	6.37 ± 0.02	6.67 ± 0.02
	5.0	7.32 ± 0.03	7.45 ± 0.03
	5.5	8.43 ± 0.04	8.65 ± 0.05
Tremblin (models)	4.0	5.52 ± 0.03	5.87 ± 0.04
	5.0	7.13 ± 0.02	7.56 ± 0.05

Next, we apply our cross correlation algorithm to our second set of thermal emission models, the four Tremblin et al. (2015) spectra. We find that, for a given surface gravity, the average line profiles

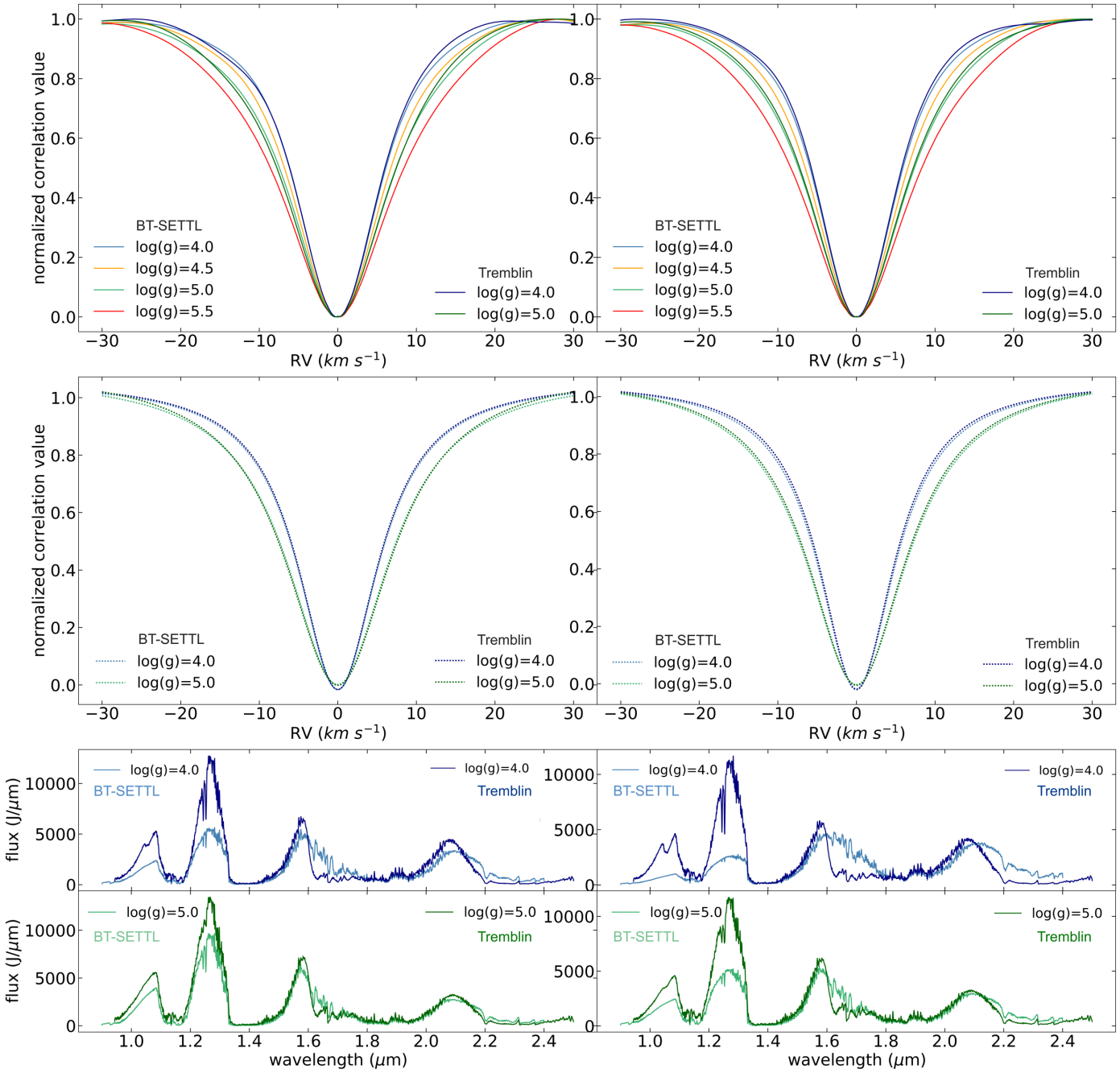

Figure 4: *Top*: The average line profiles of four PHOENIX BT-SETTL reference model spectra (light colours) and two Tremblin model spectra (dark colours) computed at BT-SETTL resolution (R=99,406). *Middle*: The Lorentzian fits of the average line profiles of two BT-SETTL reference model spectra (light green, light blue) and two Tremblin model spectra (dark green, dark blue). *Bottom*: The full flux vs. wavelength spectra (R=1000) of the models in *middle* panel. *Left*: 900 K; *Right*: 1000 K. **Main point**: Models of the same surface gravity look vastly different on the large-scale (the shape of the continuum, R=1000, *bottom* panel), but extremely similar on the small-scale (the average line profile, Reff=15,000,000, *top* and *middle* panels).

of BT-SETTL and Tremblin et al. (2015) agree remarkably well. Figure 4 shows that both the raw average line profiles and the Lorentzian fits of the Tremblin et al. (2015) models overlap with that of

the reference models for log(g)=4.0 & 5.0 at both 900 & 1000K, despite the fact that their respective spectra model shows very different atmospheres.

To emphasize this, we show the PHOENIX BT-SETTL and Tremblin et al. (2015) model spectra over the full SPIRou range, resampled to R=1000, on the same axes in the bottom panel of Figure 4.

These spectra are the same temperature and surface gravity, and yet, due to differences in how they treat important microphysical atmospheric processes affecting the shape of the continuum, they look very different. That their atmospheres are in fact experiencing the same surface gravity is apparent only when one examines the deviations from the continuum – namely the absorption lines.

CASE STUDY: 2MASS 2322-6151

In this section, we apply our method to 100 individually created simulated SPIRou observations of the Tremblin et al. (2015) model thermal emission spectra. We show the most successful of the four cases (that of log(g)=5.0, T=1000 K), noting that in two cases (log(g)=4.0, T=1000 K and log(g)=5.0, T=900 K), the average line profiles of the 100 simulated observations did not consistently align with that of the correct reference model. We scale our simulated observations to the brightness of the brown dwarf 2MASS 23225299-6151275 (hereafter 2M 2322-6151), J=13.55±0.06 mag (Cruz et al., 2009b and set the exposure time to 1. The resulting 100 spectra have a mean signal-to-noise per resolution element of ~14. We discard those flux values of the observations and reference models where observed SNR <15 or where the TAPAS telluric absorption is >0.8.

Figure 5 shows the resulting average line profiles of the 100 simulated observations and four reference models. Due to telluric absorption, our observations have only enough remaining flux values to make a stick spectrum with 605 lines, and the geometry of the average line profile suffers for it. Nevertheless, we see that the observed profiles overlap with the reference model of the same log(g) as the Tremblin model from which they were created nearly perfectly.

The small spread in the 100 simulated observations indicates that observational noise has an effect smaller than that of an object's surface gravity. Therefore, even in the presence of noise, one can measure log(g) to a better precision than 0.5 dex. As shown in Table 3, the characteristic width of the mean observed line profile, 8.34 ± 0.05 km s^{-1}, agrees with the 8.27 ± 0.02 km s^{-1} of the log(g)=5.0 reference model. By fitting a degree-3 polynomial to the four HWHM-log(g) points of the reference models (see Figure 6) and evaluating it at the HWHM of the mean observed line profile,

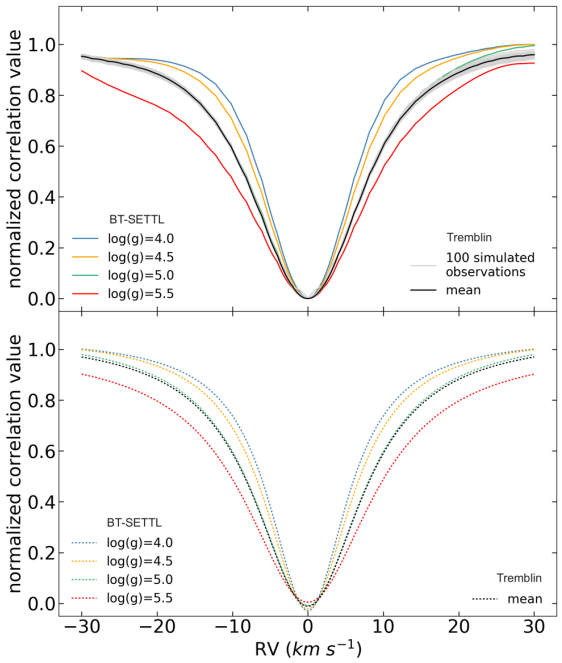

Figure 5: *Top*: The average line profiles of 100 simulated observations of the Tremblin et al. (2015) model spectrum at log(g)=5.0 and T=1000 K (grey; mean in black) and of the four BT-SETTL reference model spectra (colours). These line profiles represent the average shape of 605 individual absorption lines. *Bottom*: The Lorentzian fits of the above (observed mean only). **Main point:** The average line profile method leads us to conclude the correct surface gravity for our simulated SPIRou observations, and it is an effective way to determine surface gravity to high precision.

we obtain a surface gravity estimate of 5.015 ± 0.02 dex. In cm s^{-2}, this is a relative uncertainty of only 4.6%. Thus, not only can we recover the average line profile from observed noise, but we can compare it to reference models and conclude the correct surface gravity to high precision.

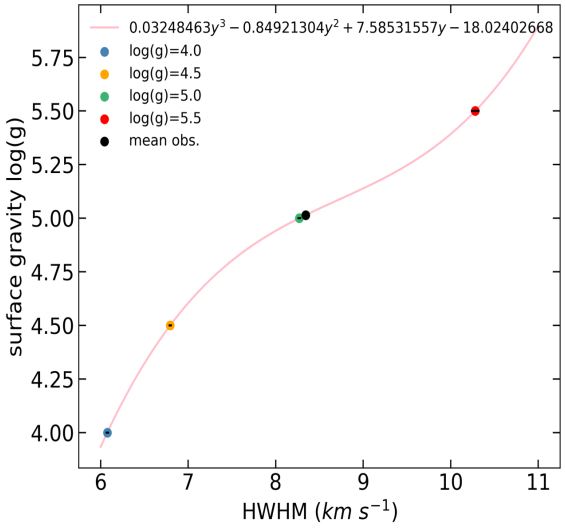

Figure 6: Empirical relationship between the characteristic width of the average line profile and the surface gravity of the model from which it is derived, found using the four reference models. The surface gravity of the mean observed line profile (black) is found to be 5.015 ± 0.02 dex. Horizontal error bars in HWHM are smaller than the width of the points.

Table 3: Characteristic widths (given by Equation 7, in km s^{-1}) of the mean of 100 simulated SPIRou observations of the Tremblin et al. (2015) model at log(*g*)=5.0 & T=1000 K, and of the Lorentzian fits to each of the four reference model spectra also at 1000 K (see Figure 5). Uncertainty in the "observed" width is the standard deviation in the characteristic width of 100 fits; uncertainties in the reference model widths were obtained with the simple variance formula.

	log(g)	HWHM
BT-Settl (reference models)	4.0	6.08 ± 0.02
	4.5	6.80 ± 0.02
	5.0	8.27 ± 0.02
	5.5	10.28 ± 0.05
Tremblin (observed)	5.0	8.34 ± 0.05

Combining this result of dg/g = 0.046 with the constraints on luminosity and temperature (dL/L = 0.03 and dT/T = 0.03) yields an uncertainty in mass of 13.7% (Equation 4).

DISCUSSION AND LIMITATIONS

Brown dwarf spectral observations made with low-resolution instruments (such as GPI, R~70) render subsequent analyses somewhat uncertain, because the method of fitting the continuum

observation to a library of model spectra could easily result in the wrong conclusion of surface gravity. That method requires the reference models to describe the same atmosphere as the observed object actually has, which is unlikely to be the case. We have shown, however, that using the spectral information present in high resolution observations made with instruments such as SPIRou and comparing average line profiles can yield the correct conclusion of surface gravity, regardless of whether the reference models correctly describe the observed atmosphere. The shape of the average spectral line in the PHOENIX BT-SETTL models, which contain clouds, is the same as that of the cloud-free models of Tremblin et al. (2015). It is remarkable that the shape of the average line would be the same for different atmospheres. Perhaps this hints at which physical process is dominant in the atmosphere.

Future work should be concerned with what is perhaps the largest caveat to this work: spectral line broadening due to the object's rotation. A fast-rotating brown dwarf's broadened spectral lines could lead it to be mistaken for an object at higher surface gravity. Efforts to decouple broadening from gravity and rotation could include an alteration to the artificial stick spectrum criteria to be sensitive to chemical species that live low in the atmosphere, and not those in the upper layers. Perhaps the mechanism-dependence of line shape could also lend itself to differentiating the effects; we have found a Lorentzian-shaped profile for non-rotating objects, whereas rotation-broadened profiles are described as a sine curve with the edges clipped due to limb-darkening. If the object's rotation speed can be constrained by some other means, then the reference model spectra can be correctly rotationally broadened and, thereon, our procedure could be applied as described. The impact of this "procedural detour" on the precision attainable would need to be studied.

More work is needed to investigate the reasons why two of the four sets of 100 simulated observations did not yield average line profiles that agreed with reference models. The procedure should also be performed with a larger variety of atmosphere models, such as the PHOENIX COND and DUSTY, to confirm the model-independence of the average line profile. Ultimately, using our method on real high-resolution spectral observations, such as those SPIRou is starting to provide, will be the definitive test for efficacy.

CONCLUSIONS

The average shape of spectral absorption lines in thermal emission spectra of brown dwarf atmospheres at different surface gravities were found to have similar shapes and be described by the same function. The characteristic width of the function, by way of our selection criteria for the artificial stick spectrum used in our cross correlation, depends on surface gravity in a simple monotonous fashion. By describing the trend with some empirical relation, we can determine the surface gravity of an object whose spectrum we observe. This work indicates that it should be possible to constrain surface gravity to better than ~5% dex using the average line profile and that this could yield mass measurements with 10-15% precision.

ACKNOWLEDGEMENTS

The authors thank both anonymous reviewers for thoughtful comments which greatly improved the manuscript. JJS acknowledges funding from iREx's Trottier Excellence Grant. We thank F. Allard et al. for making their model spectra publically available, J. Bertaux et al. for publication of their atmospheric transmission spectrum, and P. Tremblin et al. for access to their model spectra, without which this research would not be possible.

SOFTWARE

SciPy, (Jones et al. 2001); NumPy, (van der Walt et al. 2011); pandas, (Mckinney2010); Jupyter, (Kluyveretal.2016); astropy (Collaboration et al. 2013); Matplotlib (Hunter 2007).

REFERENCES

Allard, F., Homeier, D. and Freytag, B., 2012. Models of very-low-mass stars, brown dwarfs and exoplanets. *Philosophical transactions. Series A, Mathematical, physical, and engineering sciences, [online]* 370(1968), pp.2765–77. Available at: <http://www.ncbi.nlm.nih.gov/pubmed/22547243> [Accessed 8 Oct. 2018].

Artigau, É., 2018. Variability of Brown Dwarfs. [online] Available at: <https://arxiv.org/pdf/1803.07672.pdf> [Accessed 11 Sep. 2018].

Bertaux, J.L., Lallement, R., Ferron, S., Boonne, C. and Bodichon, R., 2014. TAPAS, a web-based service of atmospheric transmission computation for astronomy. *Astronomy & Astrophysics*, [online] 564, p.A46. Available at: <http://www.aanda.org/10.1051/0004-6361/201322383> [Accessed 9 Oct. 2018].

Bonnefoy, M., Chauvin, G., Lagrange, A.-M., Rojo, P., Allard, F., Pinte, C., Dumas, C. and Homeier, D., 2014. Astrophysics A library of near-infrared integral field spectra of young M-L dwarfs. A&A, [online] 562, p.127. Available at: <http://ipag.osug.fr/~gchauvin/addmaterial.html> [Accessed 4 Nov. 2018].

Bonnefoy, M., Chauvin, G., Rojo, P., Allard, F., Lagrange, A.-M., Homeier, D., Dumas, C. and Beuzit, J.-L., 2010. Near-infrared integral-field spectra of the planet/brown dwarf companion AB Pictoris b. Astronomy & Astrophysics, [online] 512, p.52. Available at: <https://www.aanda.org/articles/aa/pdf/2010/04/aa12688-09.pdf> [Accessed 4 Nov. 2018].

Bowler, B.P., Dupuy, T.J., Endl, M., Cochran, W.D., Macqueen, P.J., Fulton, B.J., Petigura, E.A., Howard, A.W., Hirsch, L., Kratter, K.M., Crepp, J.R., Biller, B.A., Johnson, M.C. and Wittenmyer, R.A., 2018. *ORBIT AND DYNAMICAL MASS OF THE LATE-T DWARF GL 758 B *.* [online] Available at: <https://arxiv.org/pdf/1802.10126.pdf> [Accessed 27 Oct. 2018].

Burrows, A., Marley, M., Hubbard, W.B., Lunine, J.I., Guillot, T., Saumon, D., Freedman, R., Sudarsky, D. and Sharp, C., 1997. A *Non-Gray Theory of Extrasolar Giant Planets and Brown Dwarfs.* [online] Available at: <https://arxiv.org/pdf/astro-ph/9705201.pdf> [Accessed 27 Oct. 2018].

Chilcote, J., Barman, T., Fitzgerald, M.P., Graham, J.R., Larkin, J.E., Macintosh, B., Bauman, B., Burrows, A.S., Cardwell, A., De Rosa, R.J., Dillon, D., Doyon, R., Dunn, J., Erikson, D., Gavel, D., Goodsell, S.J., Hartung, M., Hibon, P., Ingraham, P., Kalas, P., Konopacky, Q., Jérˆ, J., Maire, J., Marchis, F., Marley, M.S., Marois, C., Millar-Blanchaer, M., Morzinski, K., Norton, A., Oppenheimer, R., Palmer, D., Patience, J., Perrin, M., Poyneer, L., Pueyo, L., Rantakyrö, F.T., Rantakyrö, R., Sadakuni, N., Saddlemyer, L., Savransky, D., Serio, A., Sivaramakrishnan, A., Song, I., Soummer, R., Thomas, S., Wallace, J.K., Wiktorowicz, S. and Wolff, S., 2015. THE FIRST H-BAND SPECTRUM OF THE GIANT PLANET β PICTORIS b. *The Astrophysical Journal Letters*, [online] 798. Available at: <http://iopscience.iop.org/article/10.1088/2041-8205/798/1/L3/pdf> [Accessed 4 Nov. 2018].

Collaboration, A., Robitaille, T.P., Tollerud, E.J., Greenfield, P., Droettboom, M., Bray, E., Aldcroft, T., Davis, M., Ginsburg, A., Price-Whelan, A.M., Kerzendorf, W.E., Conley, A., Crighton, N., Barbary, K., Muna, D., Ferguson, H., Grollier, F., Parikh, M.M., Nair, P.H., Günther, H.M., Deil, C., Woillez, J., Conseil, S., Kramer, R., Turner, J.E.H., Singer, L., Fox, R., Weaver, B.A., Zabalza, V., Edwards, Z.I., Bostroem, K.A., Burke, D.J., Casey, A.R., Crawford, S.M., Dencheva, N., Ely, J., Jenness, T., Labrie, K., Lim, L., Pierfederici, F., Pontzen, A., Ptak, A., Refsdal, B., Servillat, M. and Streicher, O., 2013. Astrophysics Astropy: A community Python package for astronomy. A&A, [online] 558, p.33. Available at: <http://www.iausofa.org> [Accessed 8 Oct. 2018].

Cruz, K.L., Kirkpatrick, J.D. and Burgasser, A.J., 2009. YOUNG L DWARFS IDENTIFIED IN THE FIELD: A PRELIMINARY LOW-GRAVITY, OPTICAL SPECTRAL SEQUENCE FROM L0 TO L5. *The Astronomical Journal*, [online] 137, pp.3345–3357. Available at: <http://iopscience.iop.org/article/10.1088/0004-6256/137/2/3345/pdf> [Accessed 27 Oct. 2018].

Currie, T., Burrows, A., Madhusudhan, N., Fukagawa, M., Girard, J.H., Dawson, R., Murray-Clay, R., Kenyon, S., Kuchner, M., Matsumura, S., Jayawardhana, R., Chambers, J. and Bromley, B., 2013. A COMBINED VERY LARGE TELESCOPE AND GEMINI STUDY OF THE ATMOSPHERE OF THE DIRECTLY IMAGED PLANET, β PICTORIS b. *The Astrophysical Journal*, [online] 776, p.15. Available at: <http://iopscience.iop.org/article/10.1088/0004-637X/776/1/15/pdf> [Accessed 4 Nov. 2018].

Dupuy, T.J. and Liu, M.C., 2017. Individual Dynamical Masses of Ultracool Dwarfs. [online] Available at: <https://arxiv.org/pdf/1703.05775.pdf> [Accessed 27 Oct. 2018].

Dupuy, T.J., Liu, M.C., Allers, K.N., Biller, B.A., Kratter, K.M., Mann, A.W., Shkolnik, E.L., Kraus, A.L. and Best, W.M.J., 2018. *The Hawaii Infrared Parallax Program. III. 2MASS J0249−0557 c: A Wide Planetary-mass Companion to a Low-Mass Binary in the β Pic Moving Group * †.* [online] Available at: <https://arxiv.org/pdf/1807.05235.pdf> [Accessed 27 Oct. 2018].

Faherty, J.K., Riedel, A.R., Cruz, K.L., Gagne, J., Filippazzo, J.C., Lambrides, E., Fica, H., Weinberger, A., Thorstensen, J.R., Tinney, C.G., Baldassare, V., Lemonier, E. and Rice, E.L., 2016. POPULATION PROPERTIES OF BROWN DWARF ANALOGS TO EXOPLANETS. *The Astrophysical Journal Supplement Series*, [online] 225(1), p.10. Available at: <http://stacks.iop.org/0067-0049/225/i=1/a=10?key=crossref.2e5cb8a149d5e12585a1f4d1d0305b7d> [Accessed 27 Oct. 2018].

Gagné, J., Lafrenière, D., Doyon, R., Malo, L. and Artigau, É., 2014. BANYAN. II. VERY LOW MASS AND SUBSTELLAR CANDIDATE MEMBERS TO NEARBY, YOUNG KINEMATIC GROUPS WITH PREVIOUSLY KNOWN SIGNS OF YOUTH. *The Astrophysical Journal*, [online] 783(35pp), p.121. Available at: <http://iopscience.iop.org/article/10.1088/0004-637X/783/2/121/pdf> [Accessed 10 Oct. 2018].

Hedges, C. and Madhusudhan, N., 2016. Effect of pressure broadening on molecular absorption cross sections in exoplanetary atmospheres. *Monthly Notices of the Royal Astronomical Society*, [online] 458(2), pp.1427–1449. Available at: <https://academic.oup.com/mnras/article-lookup/doi/10.1093/mnras/stw278> [Accessed 27 Oct. 2018].

Homeier, D., Allard, F., Hauschildt, P.H., Barman, T.S., Schweitzer, A. and Baron, E.A., 2004. *Spectral Properties of Brown Dwarfs and Hot Jupiters.* [online] Available at: <https://arxiv.org/pdf/astro-ph/0405438.pdf> [Accessed 27 Oct. 2018].

Jones, E., Oliphant, T. and Peterson, P., 2001. {SciPy}: Open source scientific tools for {Python}.

Kluyver, T., Ragan-Kelley, B., Pérez, F., Granger, B., Bussonnier, M., Frederic, J., Kelley, K., Hamrick, J., Grout, J., Corlay, S., Ivanov, P., Avila, D., Abdalla, S., Willing, C. and Development Team, J., 2016. *Jupyter Notebooks-a publishing format for reproducible computational workeflows.* [online] Available at: <https://nbviewer.jupyter.org/,> [Accessed 8 Oct. 2018].

Marley, M.S., Jonathan Fortney, Nasa.J., Hubickyj, O., Bodenheimer, P. and Lissauer, J.J., n.d. *On the Luminosity of Young Jupiters.* [online] Available at: <https://arxiv.org/pdf/astro-ph/0609739.pdf> [Accessed 27 Oct. 2018].

Mckinney, W., 2010. Data Structures for Statistical Computing in Python. [online] *PROC. OF THE 9th PYTHON IN SCIENCE CONF.* Available at: <https://pdfs.semanticscholar.org/f6da/c1c52d3b07c993fe52513b8964f86e8fe381.pdf> [Accessed 8 Oct. 2018].

Rajan, A., Rameau, J., Rosa, R.J. De, Marley, M.S., Graham, J.R., Macintosh, B., Marois, C., Morley, C., Patience, J., Pueyo, L., Saumon, D., Ward-Duong, K., Ammons, S.M., Arriaga, P., Bailey, V.P., Barman, T., Bulger, J., Burrows, A.S., Chilcote, J., Cotten, T., Czekala, I., Doyon, R., Duchêne, G., Esposito, T.M., Fitzgerald, M.P., Follette, K.B., Fortney, J.J., Goodsell, S.J., Greenbaum, A.Z., Hibon, P., Hung, L.-W., Ingraham, P., Johnson-Groh, M., Kalas, P., Konopacky, Q., Lafrenière, D., Larkin, J.E., Maire, J., Marchis, F., Metchev, S., Millar-Blanchaer, M.A., Morzinski, K.M., Nielsen, E.L., Oppenheimer, R., Palmer, D., Patel, R.I., Perrin, M., Poyneer, L., Rantakyrö, F.T., Ruffio, J.-B., Savransky, D., Schneider, A.C., Sivaramakrishnan, A., Song, I., Soummer, R., Thomas, S., Vasisht, G., Wallace, J.K., Wang, J.J., Wiktorowicz, S. and Wolff, S., 2017. Characterizing 51 Eri b from 1 to 5 μ m: A Partly Cloudy Exoplanet. *The Astronomical Journal*, [online] 154(1), p.10. Available at: <http://stacks.iop.org/1538-3881/154/i=1/a=10?key=crossref.1003c48a2a47e76fe3105f3696486f43> [Accessed 27 Oct. 2018].

Rossow, W.B., 1978. Cloud microphysics: Analysis of the clouds of Earth, Venus, Mars and Jupiter. *Icarus*, [online] 36(1), pp.1–50. Available at: <https://www.sciencedirect.com/science/article/pii/0019103578900726> [Accessed 9 Oct. 2018].

Santamaría-Miranda, A., Cáceres, C., Schreiber, M.R., Hardy, A., Bayo, A., Parsons, S.G., Gromadzki, M. and Aguayo Villegas, A.B., 2018. Accretion signatures in the X-shooter spectrum of the substellar companion to SR12. *Monthly Notices of the Royal Astronomical Society*, [online] 475(3), pp.2994–3003. Available at: <https://academic.oup.com/mnras/article/475/3/2994/4781312> [Accessed 27 Oct. 2018].

Schneider, A.C., Windsor, J., Cushing, M.C., Kirkpatrick, J.D. and Wright, E.L., 2016. WISEA J114724.10-204021.3: A FREE-FLOATING PLANETARY MASS MEMBER OF THE TW HYA ASSOCIATION. *The Astrophysical Journal Letters*, [online] 822. Available at: <http://wise2.ipac.caltech.edu/docs/release/allwise/expsup/> [Accessed 4 Nov. 2018].

Szulágyi, J. and Mordasini, & C., 2016. *Thermodynamics of Giant Planet Formation: Shocking Hot Surfaces on Circumplanetary Disks.* [online] Mon. Not. R. Astron. Soc, Available at: <https://arxiv.org/pdf/1609.08652.pdf> [Accessed 27 Oct. 2018].

Tremblin, P., Amundsen, D.S., Chabrier, G., Baraffe, I., Drummond, B., Hinkley, S., Mourier, P. and Venot, O., 2016. *CLOUDLESS ATMOSPHERES FOR L/T DWARFS AND EXTRA-SOLAR GIANT PLANETS.* [online] Available at: <https://arxiv.org/pdf/1601.03652.pdf> [Accessed 21 Oct. 2018].

Tremblin, P., Amundsen, D.S., Mourier, P., Baraffe, I., Chabrier, G., Drummond, B., Homeier, D. and Venot, O., 2015. FINGERING CONVECTION AND CLOUDLESS MODELS FOR COOL BROWN DWARF ATMOSPHERES. *The Astrophysical Journal*, [online] 804(1), p.L17. Available at: <http://stacks.iop.org/2041-8205/804/i=1/a=L17?key=crossref.5b7cbe01d1c42a23770777627b9887bc> [Accessed 9 Oct. 2018].

van der Walt, S., Colbert, S.C. and Varoquaux, G., 2011. The NumPy Array: A Structure for Efficient Numerical Computation. *Computing in Science & Engineering*, [online] 13(2), pp.22–30. Available at: <http://ieeexplore.ieee.org/document/5725236/> [Accessed 8 Oct. 2018].

Wu, Y.-L., Close, L.M., Males, J.R., Barman, T.S., Morzinski, K.M., Follette, K.B., Bailey, V., Rodigas, T.J., Hinz, P., Puglisi, A., Xompero, M. and Briguglio, R., 2015. NEW EXTINCTION AND MASS ESTIMATES FROM OPTICAL PHOTOMETRY OF THE VERY LOW MASS BROWN DWARF COMPANION CT CHAMAELEONTIS B WITH THE MAGELLAN AO SYSTEM. *The Astrophysical Journal*, [online] 801(1), p.4. Available at: <http://stacks.iop.org/0004-637X/801/i=1/a=4?key=crossref.67a442d597c372e964e243bb86607870> [Accessed 27 Oct. 2018].